ΠΑΝΕΠΙΣΤΗΜΙΟ ΚΡΗΤΗΣ

ΤΜΗΜΑ ΦΥΣΙΚΗΣ

ΠΤΥΧΙΑΚΗ ΕΡΓΑΣΙΑ

THEORETICAL MODELLING OF AGN OPTICAL VARIABILITY

ΦΟΙΤΗΤΗΣ: ΑΥΓΟΥΣΤΑΚΗΣ ΙΩΑΝΝΗΣ (Α.Μ. 4108)

ΕΠΙΒΛΕΠΩΝ ΚΑΘΗΓΗΤΗΣ: ΠΑΠΑΔΑΚΗΣ ΙΩΣΗΦ

ΗΡΑΚΛΕΙΟ, ΙΟΥΛΙΟΣ 2018

CHAPTER 1:
INTRODUCTION

1.1 Definition of AGN and their characteristics

We call “Active Galactic Nuclei” (AGN) the central parts of some galaxies (~10% of the galaxies in the near Universe) when the light they emit cannot be attributed to normal stellar processes. The non stellar origin of their emission has become the reason for increased scientific interest over the last decades. The following are their most common observational characteristics:

-Bright star-like nucleus: Active galaxies have a point-like source at their center which radiates power that can be higher than the rest of the galaxy. For example, AGN bolometric luminosity can some times exceed 10^{45} *erg/s* while the typical luminosity of normal galaxies is of the order of 10^{44} *erg/s*.

-Wide spectrum continuum emission: For most normal galaxies, their spectrum is mostly the sum of the spectra of the stars consisting the galaxy. Star spectra are approximately black body spectra. M stars have temperatures between 2400 and 3700 *K* and the hotter A stars have temperatures between 7500 and 10000 *K*. This implies that these stars emit most of their radiation at wavelengths between 2 and 300 *nm*, which ranges between the near infrared (NIR) and near ultra violet (NUV) regions of the electromagnetic spectrum. As a result, this is the band where most of the light from normal galaxies is emitted. The hottest O and B stars don't contribute significantly to the UV region of the galactic spectrum, since the population of such stars is much smaller than the population of smaller and cooler stars (like A, F, G etc.). Because of this, we observe a strong cut-off in the UV region of the galactic spectra. On the other hand, AGN emit (approximately the same) power over a wide range of frequencies, from radio up to gamma rays (see Fig. (1.1)). In addition, the AGN spectrum increases as we move to ultraviolet wavelengths, in strong contrast to the normal galaxy. These two characteristics of the AGN (i.e. the wide spectral range emission and the UV excess) can not be explained by stellar processes.

-Strong emission lines: Typical galactic spectra show strong absorption lines and faint emission lines. The absorption lines originate from the ionization of elements such as H, O, Si, He, etc. in the stellar atmospheres. On the other hand, AGN show strong emission lines in their optical spectra. Two kinds of emission lines can appear. The first, produced by low density ionized gas ($n_e \approx 10^3 - 10^6 cm^{-3}$) are characterized by velocities of several hundred up to 2000 *km/s*. The second set originates from higher density gas ($n_e \approx 10^9 cm^{-3}$). The characteristic velocities of these lines can be up to 10000 *km/s*. AGN that show both broad and narrow lines are categorized as Type 1, while those that show only narrow lines are called Type 2.

-Radio loudness: Some AGN (about 10% of all AGN) show strong radio emission. These objects are characterized by the “radio-loudness”, i.e. the ratio of the radio band flux at $5 GHz$ over the optical band flux at *B*-band. If this ratio is greater than 10, the AGN is considered as “radio-loud”.

-Strong variability: A major characteristic of AGN emission is that their flux is variable on both short (hours, days) and long (weeks, months, years) timescales. The variability amplitude decreases with increasing wavelength. At optical bands, luminosity changes of ~10% (and more) are observed at weekly, monthly, and yearly timescales. In contrast, the X-ray flux can vary significantly (by a factor of 2, or more) on timescales as short as a few minutes to an hour.

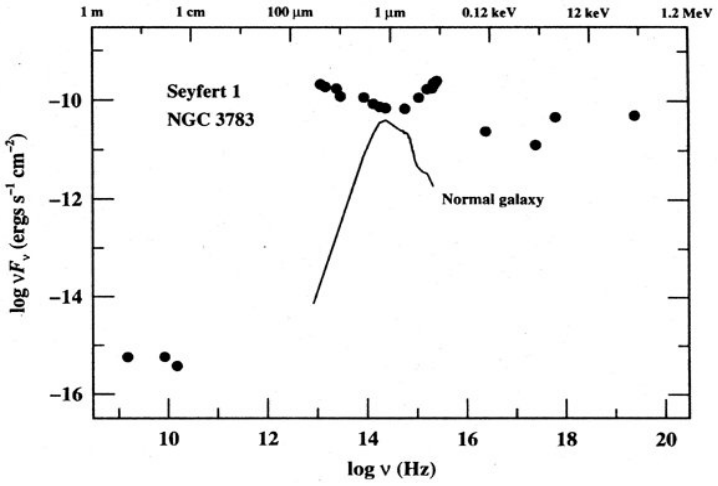

Fig. 1.1 Comparison between the broad band spectrum of NGC 3783 (filled dots), which hosts an active nucleus, and the spectrum of a normal galaxy spectrum (solid line).

1.2 Current paradigm

Today, we believe that AGN consist of a supermassive black hole surrounded by an accretion disc. The disc rotates differentially, and matter at shorter radii rotates faster compared to that at larger radii. Viscous forces between disc rings of different radii cause loss of angular momentum. Consequently, matter in the disc moves inwards, towards the black hole and thus, gravitational potential energy is released. This energy heats up the disc, increasing its temperature and the disc radiates as a multi-colour black body. This mechanism can explain the strong optical/UV emission of AGN, as well as their large luminosity, provided that the central black hole has a mass is of the order of (many) million solar masses.

To show that this is the case, let us assume spherical distribution of matter surrounding a body of mass *M*. We also assume that matter around the central object consists only of totally ionized hydrogen gas that falls constantly on the central object. As matter falls towards the center, potential energy is released. Let us assume that, in some way, this liberated energy is transformed into radiation that is emitted from the center. The outward radiated energy flow at distance R from the center is

$$f = \frac{L}{4\pi R^2} \quad . \qquad (1.1)$$

The radiation pressure on the gas particles will be

$$P_{rad} = \frac{f}{c} = \frac{L}{4\pi c R^2} \quad . \qquad (1.2)$$

The radiation pressure acts a force on both electrons and protons is given by:

$$F_{rad} = \sigma \frac{L}{4\pi c R^2} r \quad , \quad (1.3)$$

where $\sigma = \frac{8\pi}{3}\left(e^2/mc^2\right)^2$ is the Thomson scattering section.

Since the proton is much heavier than the electron, σ_P is much lower (because $\sigma_P \sim m^{-2}$) thus, the force acting on the protons is much weaker than the force acting on the electrons. F_{rad} has obviously an outward direction, opposite to the gravitational force which acts inwards, towards the center. The gravitational force acting on electrons and protons is:

$$F_{grav} = GM\frac{(m_p + m_e)}{R^2} \approx \frac{GMm_p}{R^2} \quad . \quad (1.4)$$

Clearly, the source luminosity must be such that $F_{rad} \le F_{grav}$. Otherwise, the outward force will be larger than gravity. In this case, accretion will stop and hence the source will not emit anymore (assuming that the only source of power is the release of gravitational potential energy, as the particle falls towards the central object). In the case when $F_{rad} = F_{grav}$, the source will emit with maximum luminosity, L_E, known as the Eddington limit. So, equating (1.3) with (1.4), we get

$$F_{rad} = F_{grav} \Rightarrow \sigma_e \frac{L}{4\pi c R^2} = \frac{GMm_p}{R^2} \Rightarrow L = 4\pi c \frac{Gm_p}{\sigma_e} M = 6.31 \times 10^4 M \Rightarrow L_E = 1.26 \times 10^{38} \left(\frac{M}{M_{Sun}}\right)(erg/s) \quad . \quad (1.5)$$

The Eddington luminosity, when combined with the observed bolometric luminosity of AGN can constrain *M*. Indeed, if an AGN accretes at the Eddington limit, it is relatively easy to show that it's mass must be at least equal to M_E, where

$$M_E = 8 \times 10^5 L_{44} M_{Sun} \quad . \quad (1.6)$$

L_{44} is the luminosity of the source measured in units of 10^{44} *erg/s*. For an observed bolometric luminosity of $L_{bol} \simeq 100 L_{44}$, eq. (1.6) yields that $M_E \simeq 8 \times 10^7 M_{Sun}$. Therefore, for the luminous AGN, we expect their mass to be least $\sim 10^8 M_{Sun}$ (otherwise, their observed bolometric luminosity would significantly exceed their Eddington limit).

One could assume that the central gravitational source is a dense star cluster consisting of 10^8 Sun-like stars. However, AGN vary significantly in short timescales. In general, the flux of a source can not vary much faster than the time interval, Δt, required for the light to travel across the volume of that source. So, for a source with variable flux, the characteristic size must be smaller than $l \sim c\Delta t$, where Δt is the time interval over which the flux varies by a factor of ~2, at least. X-rays from AGN can vary by a factor of two, or more, within an hour. Therefore, $R_{cluster} \sim 10^{14} cm$. This radius is smaller than the radius of our solar system, meaning that, if there is a dense cluster in the central region of AGN, $\sim 10^8$ Suns must be placed inside a volume of that size. This configuration of stars must be dynamically unstable and should collapse to a supermassive black hole.

1.3 AGN optical variability

The AGN flux is variable at all wavelengths. The amplitude of their optical variability is of the order of several tenths of a magnitude in timescales of months and years (e.g. Giveon et al. 1999; Vanden Berk et al. 2004). Figure (1.2) shows the optical lightcurves of some AGN observed in a total period of 7 years from March 1991 to March 1998 in the Johnson-Cousins *B* and *R* bands (empty and filled symbols, respectively). The uncertainty of the observations is ~0.01 mag in the *R* band, while the uncertainty is higher in the *B* band (~0.02 mag), due to the lower CCD sensitivity in the blue light. The lightcurves plotted in Fig. (1.2) show that the variations are random, with a max-to-min variation of the order of ~0.2 – 0.8 mag for most objects.

Dependence on luminosity: The amplitude of the optical variability, on timescales of years, appears to be anti correlated with luminosity (Hook et al. 1994; Giveon et al. 1999; Vanden Berk et al. 2004; Wilhite et al. 2008; Bauer et al. 2009; MacLeod et al.2010; Zuo et al. 2012). Figure (1.3) shows a plot of the *R* band variability amplitude vs the rest-frame *R* band luminosity. Filled symbols show radio quiet sources while open symbols show radio loud sources. The *R* band variability amplitude (measured with the standard deviation of the observed lightcuves, σ) appears to decrease with increasing luminosity. This result indicates that more luminous objects are less variable.

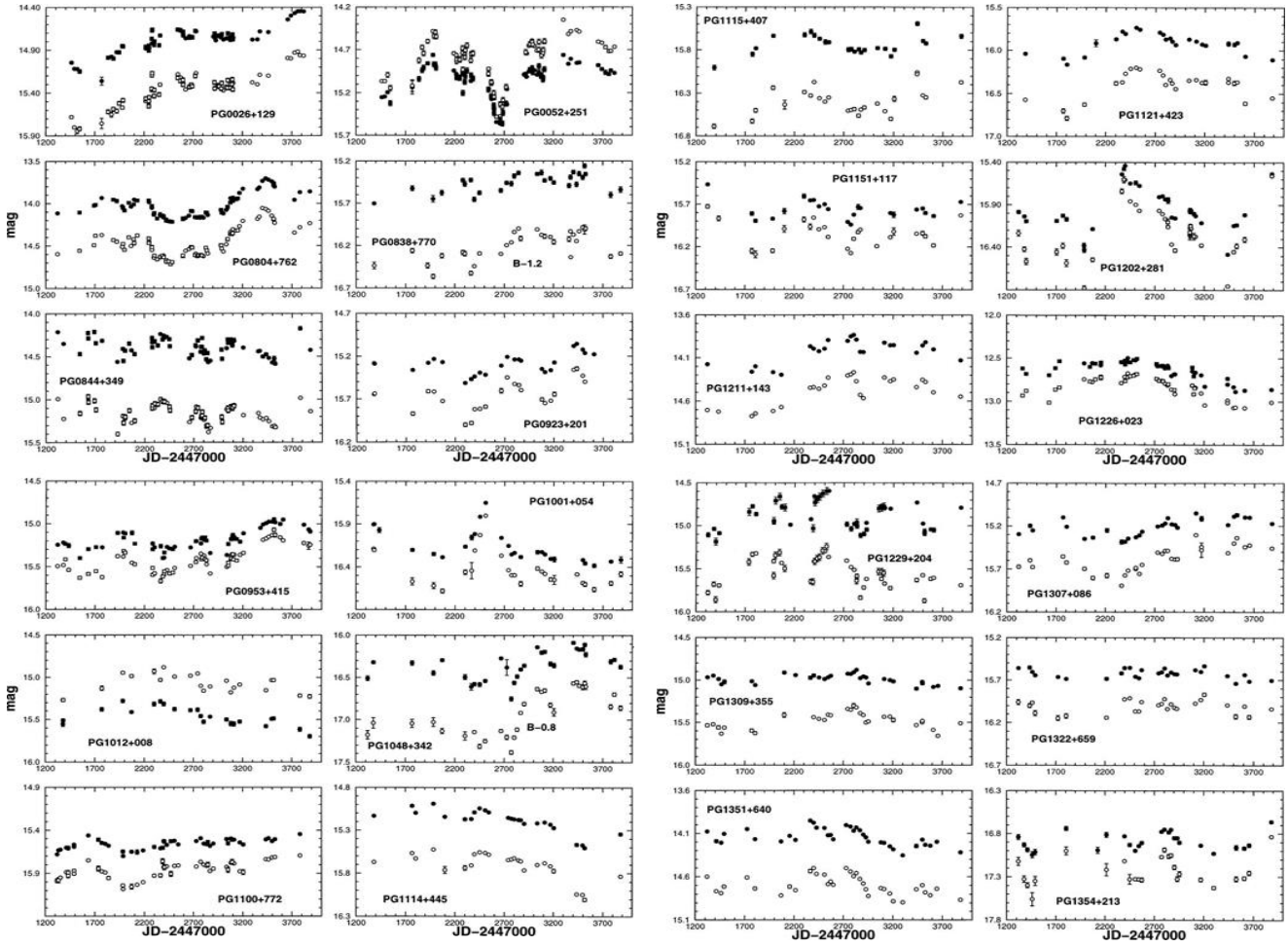

Fig. 1.2 Optical lightcurve of several AGN in the *R* and *B* bands (filled and empty dots, respectively; Giveon et al. (1999)).

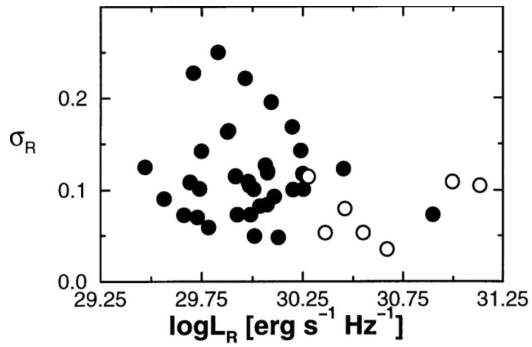

Fig. 1.3 *R* band variability amplitude vs the rest-frame *R* band luminosity (Giveon et al. 1999). Radio quiet and radio loud sources are plotted with filled and empty symbols respectively.

Dependence on black hole mass: There is a discrepancy between the observations of several authors regarding the dependence of variability amplitude on black hole mass. Some of them find a positive correlation, while others observe negative or even no correlation on similar variability timescales (Wold et al. 2007; Wilhite et al. 2008; MacLeod et al. 2010; Zuo et al. 2012). Left panels in Fig. (1.4) show plots between the excess variance (i.e. the variance after subtracting the variance due to observational errors) of optical lightcurves and the black hole mass for a large sample of AGN. The figure is taken from Simm et al. (2016). These authors have studied the optical variability of AGN selected from the XMM-COSMOS survey using data from the Pan-STARRS 1 telescope which is located in Haleakala Observatory in Hawaii, USA. The telescope has a 1.8m primary mirror and a 0.9m secondary mirror. A 1.4 *gigapixel* camera (GPC1) is mounted on the telescope. The sensor of this camera is a mosaic that consists of 60 CCD chips with a resolution of 4800X4800 pixels each. Approximately 180 – 130 AGN in the COSMOS field were observed with this telescope using 5 filters, namely g_{P1}, r_{P1}, i_{P1}, z_{P1}, w_{P1}. These are SDSS-like filters with some minor differences (the response curves of the g_{P1}, r_{P1}, i_{P1}, z_{P1} filters are shown in Fig. (3.2). The observations were done in a period of ~4 years from ~ November of 2009 to ~ February of 2014.

Simm et al. (2016) used ~3 years and 3-4 months long lightcurves to measure the optical variability amplitude on long and short time scales. The top left panel in Fig. (1.4) suggests that there is no correlation between the excess variance and the black hole mass on long time scales. The bottom left panel shows that there may be a weak anti-correlation between the excess variance and the black holes mass on shorter time scales. However, Simm et. al (2016) found that this is is not statistically significant.

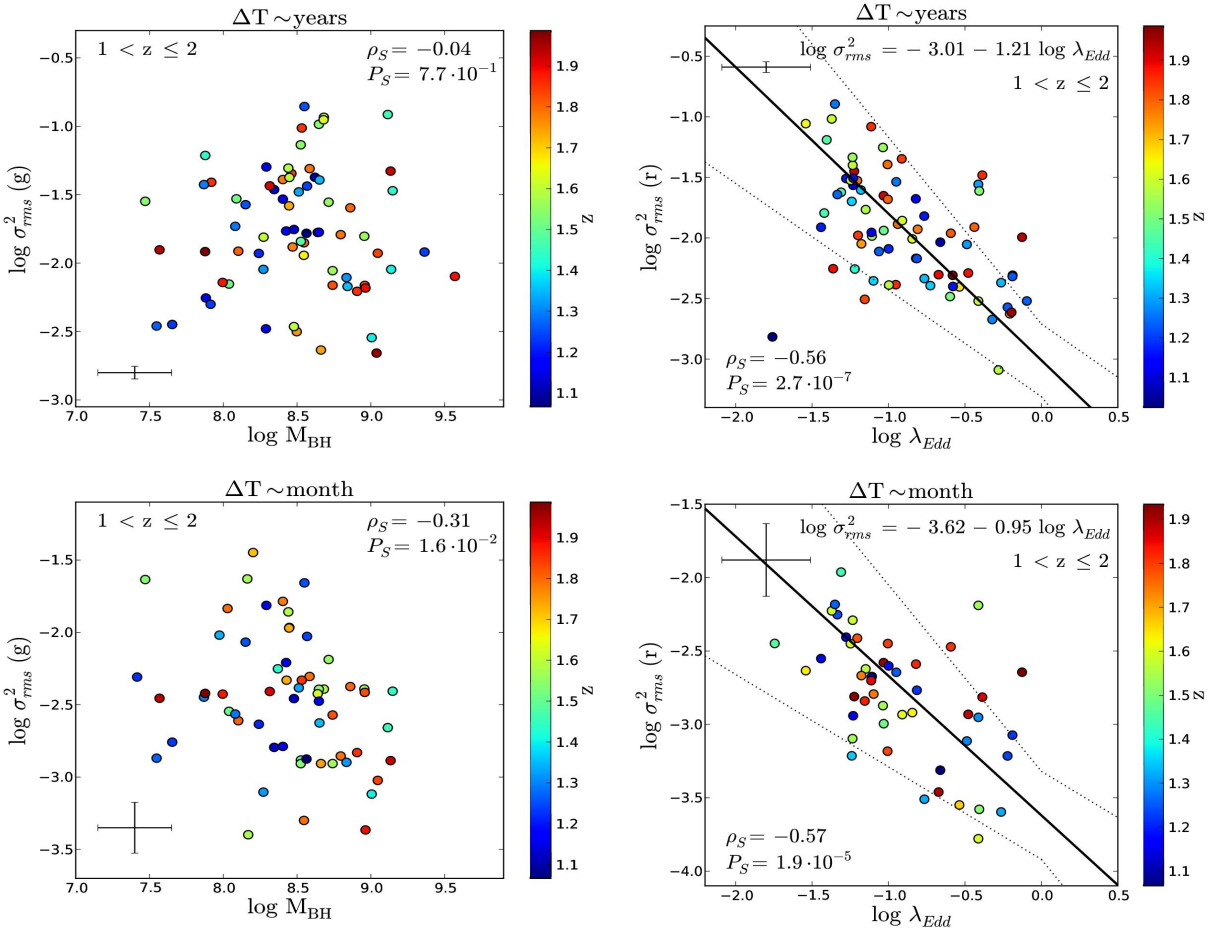

Fig. 1.4 Optical variability amplitude versus the black hole mass and the accretion rate in left and right panels respectively. Figures taken from (Simm et al. 2016).

Dependence on accretion rate: According to the current paradigm, as long as the main source of power in AGN is the release of gravitational potential energy as matter falls to the central black hole, their bolometric luminosity should be given by: $L_{bol}=\varepsilon\cdot\dot{M}c^2$, where ε is the efficiency of the conversion of the gravitational power to radiation, and $\dot{M}$ is the so called accretion rate, i.e. the rate with which matter falls towards the black hole. The Eddington accretion limit, $\dot{M}_E$, is the accretion rate that is necessary for the object to radiate at the Eddington luminosity (L_E), i.e.: $L_E=\varepsilon\cdot\dot{M}_E c^2$, . The ratio $\lambda_E=\frac{\dot{M}}{\dot{M}_E}=\frac{L_{bol}}{L_E}=\dot{m}$ gives the accretion rate in units of $\dot{M}_E$ and is called the "Eddingtion ratio" of an AGN. It is an important physical parameter of the system.

Several authors observe an anti-correlation between optical variability and Eddington ratio on long and short timescales (Wilhite et al. 2008; Bauer et al. 2009; Ai et al. 2010; MacLeod et al. 2010; Zuo et al. 2012),. The right panels of Fig. (1.4) show the optical excess variance vs the Eddington ratio (Simm et al. 2016). The same sources appear in the plots in left panels and in the right panels of Fig. (1.4). The plots in the left panels show no correlation between the variability amplitude and the black hole mass. On the contrary, the plots in the right panels show a strong anti-correlation between the variability amplitude and mass accretion rate. According to these results, Simm et al. (2016) conclude that the optical variability amplitude of AGN is independent of the black hole mass, but it decreases as the mass accretion rate increases.

The optical variability at various wavelengths: As already said, the variability amplitude decreases towards longer wavelengths. This is also the case within the optical/UV band. Due to the intense monitoring of a few AGN during the last few years, it has been possible to study in detail their variability at various wavelengths within the optical/UV band. Figure (1.5) (Edelson et al. 2015) shows the lightcurves of NGC 5548, based on observations by the *Swift* Observatory and Hubble Space Telescope (HST). The observations were very intense and lasted for ~4 months, from March to June 2014. The 2 top panels show the lightcurves in the X-ray band (from 25 *Å* to 4.4 *Å*). The rest of the panels show the optical/UV lightcurves of the same AGN from *V* band (5468 *Å*), to the far UV (1367 *Å*).

Figure (1.5) shows that the optical/UV lightcurves follow the same pattern of variability. The amplitude of the variations increases as we move from larger (e.g. *V* band) to smaller wavelengths (e.g. X-rays). Also, the timescale of the variations decreases with decreasing wavelengths. The variations in X-ray band are far more rapid than the variations in the optical/UV bands, indicating that the X-ray source should be very close to the black hole. The peaks of two flare-like events that appear in the optical/UV bands (indicated by the left and right vertical dashed line) do not appear to be completely lined up between lightcurves of different wavelengths. There is a time lag of ~2 *days* between the peak in the 1367 and 5468 *Å*.

These delays can be explained by the so called "X-ray reprocessing" scenario. According to this model, a fluctuating X-ray source emits radiation that illuminates the disc. An accretion disc of constant temperature, with respect to time, absorbs the X-ray radiation which causes further heating. The region of the disc closer to the X-ray source is heated more than the regions further away from the source (the X-ray source is assumed to radiate isotropically and is close on top of the black hole). Variations in the X-ray source cause variations in the heating rate of the different, illuminated regions of the disc. This, in turn causes variations in the temperature of these regions. Since the region of UV emission is closer to the X-ray source, it will respond to the X-ray variations earlier than the optical emission regions. This should introduce time lags (i.e. delays) between the variations in the UV and optical bands.

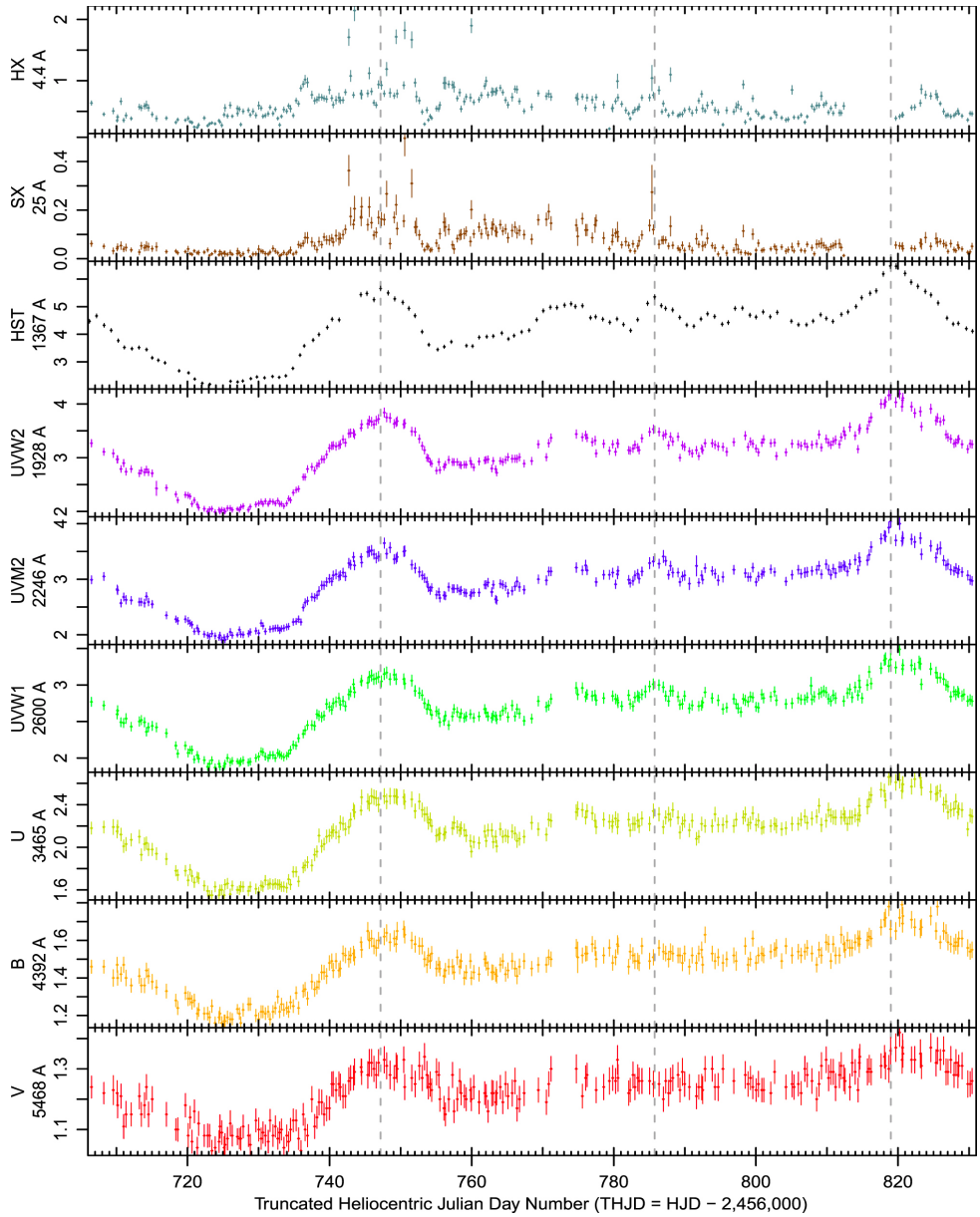

Fig. 1.5 Optical/UV/X-ray lightcurves of NGC 5548 based on Swift and HST observations. Units are in *counst/s*, except the third panel, which shows the HST lightcurve in units of $10^{-14}\, ergs \cdot cm^{-2} s^{-1}$ $Å^{-1}$ (Edelson et al. 2015).

1.5 Objective of the present work

In this work I study a particular theoretical model for the AGN variability that was first introduced by Lyubarskii (1997) [see also Arevalo & Uttley, 2006 (AU06 hereafter) and Ingram & Done, 2011 (ID11 hereafter)]. According to this model, the accretion disc is affected by local accretion rate fluctuations, whose characteristic time-scale is of the order of the local viscous time-scale (I will define this time scale in the next Chapter). The fluctuations at different radii are uncorrelated but propagate inwards, modulating the emission of the inner regions with long term variations.

Since the accretion disc temperature, *T(R)*, depends on $\dot{M}$ (as it is shown in Chapter 2), if such fluctuations operate, whose flux depends on *T(R)*, the $\dot{M}$ variations will eventually produce flux variations.

The main objective of the present work is to develop a code that will produce variations in the flux of the emitted radiation from an accretion disc that surrounds a black hole of mass M_{BH}, in the of the “propagating fluctuations” model. The main parameters that characterize the system are:

1.) The mass of the black hole, M_{BH}
2.) The mean mass accretion rate, $\dot{m}$ (in Eddington units)
3.) The amplitude of mass accretion rate fluctuations.

The code, using as main input the above parameters, calculates the mass accretion rate fluctuations at a set of points, over a period of time. It also takes into account that these fluctuations propagate inwards causing variations of mass accretion rate at all radii. Then, it calculates the temperature profile of the accretion disc (as a function of time), which depends on the mass accretion rate. Since the accretion disc emits black body radiation (as it is optically thick according to the thin disc approximation), the code then calculates the luminosity variations of the whole disc as a function of time (i.e. the total lightcurve).

CHAPTER 2:
ACCRETION DISC MODELING

In many astrophysical phenomena, such as X-ray binaries and AGN, it is widely believed that matter is rotating around a central, compact object. Closed orbits around the central object, originally inclined one another, will eventually collide in the plane of intersection and the angular momentum of those particles mix. Angular momenta of all particles will combine into a total angular momentum and thus all orbits will be on the same plane, perpendicular to the angular momentum vector, forming a disc.

In the modeling bellow, I will follow the thin disc approximation, assuming that the disc is geometrically thin. This means that the height of the disc at radius *R*, *H(R)*, is much smaller than *R*. I also assume that the gravitational potential at each radius is mostly dominated by M_{BH}. As a result, the azimuthal rotation of the gas around the black hole will follow a circular Keplerian motion, so that:

$$\upsilon_{\varphi}(R)=\omega_{\kappa}(R)\cdot R=\left(\frac{GM_{BH}}{R}\right)^{1/2} \quad , \quad (2.1)$$

where $\omega_k(R)$ is the Keplerian angular frequency. The specific angular momentum, which is the angular momentum per unit mass, is given by:

$$l(R)=R\upsilon_{\varphi}=\sqrt{GM_{BH}R} \quad . \quad (2.2)$$

As a particle moves inwards, closer to the black hole (i.e. as *R* decreases), υ_{Φ} increases but *l(r)* decreases. So, particles further out have larger angular momentum than particles closer to the black hole. Therefore, a particle needs to lose angular momentum to move closer to the black hole and fall in. This can be achieved by the action of stresses between neighbouring rings which rotate at different angular velocities.

2.1 The temperature profile of the accretion disc

Let us consider two rings of gas at radii *R* and $R+\Delta R$. As the rings follow Keplerian motion, the inner one rotates faster than the outer. As a result of the viscous stress, the inner ring slows down and loses angular momentum. Most of the gas occupying the ring will eventually move further inward, closer to the black hole, while the remaining will move outward, carrying with it the excess angular momentum.

The subsequent inward motion of the gas leads to gravitational potential energy dissipation. According to the virial theorem, half of the potential energy that is released becomes kinetic energy, while the other half turns into internal energy. For a mass *m* moving from *R* to $R+\Delta R$, the released potential energy is given by

$$\Delta E=\frac{GM_{BH}m}{R}-\frac{GM_{BH}m}{R+\Delta R}\approx\frac{GM_{BH}m\Delta R}{R^2} \quad . \quad (2.3)$$

Therefore, the increase of internal energy of the particles in the ring is $\Delta U=\Delta E/2$. We assume that this energy is dissipated locally into heat, increasing the ring temperature. If matter accretes at a rate of $\dot{M}=dM/dt$, then the heating rate of the ring, Q_{in}, will be:

$$Q_{in}=\frac{GM_{BH}\dot{M}}{2R^2}\Delta R \quad . \ (2.4)$$

If the disc is dense enough to be optically thick, (i.e. the mean free path of the photons is too small, so that the photon gas and matter are in thermal equilibrium) then every segment of the disc will radiate as a black body. If that is the case, for a ring between R and $R+\Delta R$, the amount of energy emitted per unit time (i.e. the emitted power) will be:

$$Q_{out}=2\cdot 2\pi R\Delta R\sigma_{SB}T(R)^4 \ , \ (2.5)$$

where $T(R)$ is the ring temperature and σ_{SB} is the Stefan-Boltzmann constant (the factor 2 comes from the fact that the disc emits from both sides). By combining the above two equations we can solve for the radial dependence of the temperature:

$$T(R)=\left(\frac{GM_{BH}\dot{M}}{8\pi\sigma_{SB}R^3}\right)^{1/4} \quad . \ (2.6)$$

A more careful derivation, with a proper modeling of the torques between neighboring rings, one obtains the following relation (Pringle, 1981):

$$T=\left[\frac{3GM\dot{M}}{8\pi R^3\sigma}\left(1-\sqrt{\frac{R_{in}}{R}}\right)\right]^{1/4} \ ,$$

where R_{in} is the inner radius of the disc. This equation is valid under the assumption that the torque at $R=R_{in}$ vanishes. The above equation can also be written as follows,

$$T=1.86\times 10^6\left[\frac{\dot{m}}{m_7}r^{-3}\left(1-\sqrt{\frac{r_{in}}{r}}\right)\right]^{1/4} \ (K) \ , (2.7)$$

where $m_7=M_{BH}/10^7 M_{Sun}, M_{Sun}=2\times 10^{30}kgr$, radii are measured in units of the gravitational radius r_g (i.e. $r=R/r_g$, where $r_g = GM/c^2$), and the accretion rate is measured in units of the Eddington accretion rate (i.e. $\dot{M}_{Edd}=\varepsilon L_{Edd}$, where ε is the accretion efficiency, and have I assumed that $\varepsilon=0.1$).

2.2 The emitted spectrum

Knowing $T(R)$ and assuming that the disc emits locally as a black body, then the flux of a disc ring at temperature T will be :

$$F_\lambda(\lambda,R)=\frac{2\pi hc^2}{\lambda^5}\frac{1}{\exp[hc/\lambda k_B T(R)]-1} \quad (W/m^2/wavelength). \ (2.8)$$

Consequently, the flux of the whole disc, F_λ, at a given wavelength, λ, will be equal to:

$$F_\lambda=\int_{R_{min}}^{R_{max}} F_\lambda(\lambda,R)2\pi R dR \quad (W/wavelength), \ (2.9)$$

where h is the Planck constant, c is the light speed and k_B is the Boltzmann constant.

2.3 Variability timescales of the Keplerian accretion flow

Below, I discuss the main variability timescales for a Keplerian, optically thick, geometrically thin accretion disc. These characteristic timescales are functions of the accretion disc radius and other parameters, such as M_{BH} , the viscosity parameter, α, and the disc thickness $H(R)$.

2.3.1 The dynamical timescale

If the flow of the gas in the accretion disc follows a Keplerian orbit, then the dynamical timescale of the disc is given by the period corresponding to the Keplerian frequency (Czerny, 2006):

$$t_{dyn}(R)=\sqrt{\frac{R^3}{GM_{BH}}}=166.7\,r^{3/2}m_7 \quad (s). \quad (2.10)$$

This time scale is equal to the characteristic time of the motion of a particle at a circular orbit (i.e. the local rotation period of the accretion disc) and it is of the same order of magnitude as the free-fall timescale.

The disc emission can be variable on $t_{dyn}(R)$. For example, if the disc is inhomogeneous, and some parts of the disc are hotter then the rest, their rotation could cause variations in the emitted flux due to Doppler-boosting effects. The disc part that moves away from the observer emits radiation at lower frequencies, while the disc part that moves closer to the observer emits radiation at higher frequencies. Since the observer measures the radiation flux at a specific frequency, they will observe flux variations as the maximum of the radiation flux emitted from some parts of the disc varies periodically from lower to higher frequencies and vice versa.

2.3.2 The thermal timescale

The thermal timescale, $t_{th}(r)$, is defined as the ratio of the internal energy of the disc over the cooling or heating rate of the disc. This timescale is representative of the time it takes for the disc to reach local thermal equilibrium. The thermal energy absorbed by a disc ring at radius R, per unit time, should be equal to the power emitted as radiation from the same part of the disc. If there is a variation in either the cooling or heating rate, and hence a variation of the local temperature, the thermal timescale indicates the time it takes for a part of the disc to reach the equilibrium temperature $T(R)$ as given in equation (2.7). Assuming that the disc viscosity is described by the parameter α (Shakura & Sunyaev, 1973), known as the viscosity parameter[1], $t_{th}(r)$ can be related to the characteristic dynamical timescale as (Czerny, 2006):

$$t_{th}(r)=\alpha^{-1}t_{dyn}(r)=1.66\times10^{3}\,r^{3/2}m_7 \quad (s), \quad (2.11)$$

where I assumed that $\alpha=0.1$. The thermal timescale is independent of the cooling or heating mechanism and the optical depth. Therefore, the thermal timescale will be the same for a cold, optically thick disc and a hot, optically thin disc.

[1] This parameter characterizes the efficiency of the mechanism for angular momentum transfer.

2.3.3 The viscous timescale

The viscous timescale, $t_{visc}(r)$, is representative of the characteristic time of the accreting mass flow. It is defined as the ratio of the accretion disc radius over the radial velocity of the accretion flow. In the case of a mass accretion rate fluctuation, the surface density of the accretion disc gas will change. This time scale is representative of the time it takes for the disc surface density to reach the equilibrium value in this case. The viscous timescale can be related to the thermal timescale as (Czerny, 2006):

$$t_{visc}(r)=t_{th}(r)[\frac{r}{H(r)}]^2 \quad (s). \quad (2.12)$$

For a hot and optically thin disc, where the temperature reaches the virial temperature (i.e. the temperature at which a gravitationally bound system, such as the accretion disc around a compact central object, satisfies the virial theorem) the ratio $r/H(r)$ is close to 1. In that case, the viscous timescale is equal to $t_{th}(r)$. In the case of a cold and optically-thick accretion disc, the ratio $r/H(r)$ is large, so the viscous timescale is orders of magnitude larger than $t_{th}(r)$. Assuming a typical value of $r/H(r)=10$ in eq. (2.12), and combining it with eq. (2.11), we get:

$$t_{visc}(r)=1.66\times10^5 r^{3/2} m_7 \quad (s). \quad (2.13)$$

2.4 The variability model of mass accretion fluctuations

Let us assume a standard, geometrically thin, optically thick accretion disc, around a Schwartzchild black hole (i.e a non rotating black hole), with R_{in} equal to the radius of the innermost circular stable orbit (ISCO) of the disc (which, in this case it is equal to $3R_s$, where $R_S=\frac{2M_{BH}G}{c^2}=2r_g$, is the Schwarzschild radius). Let us suppose that the local mass accretion rate at a radius r, fluctuates around a mean value of $\dot{M}_0(r,t)$ as follows:

$$\dot{M}(r,t)=\dot{M}_0(r,t)\dot{m}(r,t) \quad . \quad (2.14)$$

If that is the case, let us now also assume that the accretion rate fluctuations propagate inward and $\dot{M}(r,t)$ will serve as $\dot{M}_0(r',t')$ for the fluctuation produced at an inner ring, r', at a later time, t'. Here, t'-t is the time interval needed for the fluctuation to move from r to r' (where $r'<r$).The fluctuations propagate inwards with a propagation speed equal to the local radial drift velocity, $\upsilon_r(r)$:

$$\upsilon_r(r)=r^{-1/2}(H/R)^2 a \quad . \quad (2.15).$$

The mass accretion rate fluctuations, $\dot{m}(r,t)$, are random. Their mean value is equal to one (i.e. $<\dot{m}(r,t)>=1$) and their amplitude is expected to be small (i.e. $\Delta\dot{m}(r,t)\ll1$). Two major properties of a random process are the variance, σ^2, and the so called "power spectrum density function" or simply "power spectrum", $PSD(f)$. The variance determines the average spread of the random values of the process around their mean value (i.e. the "central value" of the process). The power spectrum, which is a function of frequency, has the following property:

$$\int_{-\infty}^{+\infty} PSD(f)\,df=\sigma^2 \quad . \quad (2.16)$$

The meaning of the above equation is as follows: let us decompose the random process in a series of harmonic waves, each with a frequency of *f*. Broadly speaking, on average, the contribution of each of these waves to the total variance of the process will be equal to the power spectrum density multiplied by the frequency. So, in a way, the power spectrum determines the amplitude of these waves, and of the variability process in general.

Regarding $\dot{m}(r,t)$ we will follow AU06 and ID11, and we assume that the accretion rate fluctuations should operate mostly at the local viscous time scale, and that their power spectrum follows a zero centered Lorentzian function, cutting off at the viscous frequency, i.e.

$$PSD_{\dot{m}}(r,f)=\frac{1}{1+\left[\frac{f}{f_{visc}(r)}\right]^2} \quad , (2.17)$$

where

$$f_{visc}(r)=\frac{1}{t_{visc}(r)}(Hz) \quad (2.18)$$

is the viscous frequency at distance *r*.

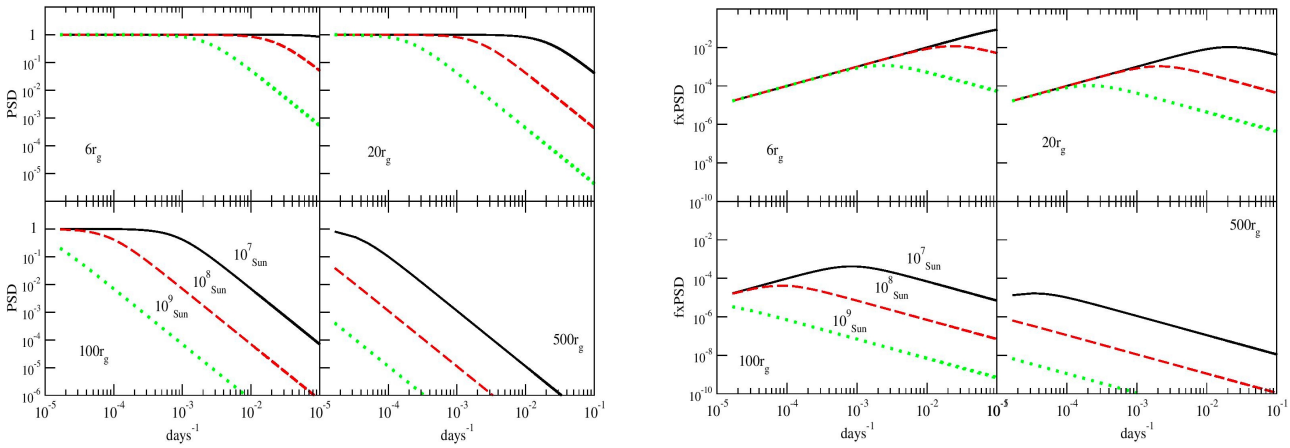

Fig. 2.1, (***left)***: Theoretical power spectrum of mass accretion rate fluctuations at various distances from the center for three different M_{BH} (dotted dashed and solid lines for 10^7, 10^8, 10^9 M_{Sun})
Fig. 2.1, (***right)***: *f*PSD* as function of frequency, for the same plots shown in the left panel.

The left panel in Fig. (2.1) shows the model *PSD(f)* of the fluctuations at various distances from the central black hole in the case when $M_{BH} = 10^7$, 10^8 and 10^9 M_{sun} (dotted, dashed and solid lines respectively). The *PSD* is flat at frequencies lower than the viscous frequency at each radius.

The right panel in the same figure, shows a plot of the product *f*PSD* vs frequency. This product represents the contribution of the Fourier components of frequency *f* to the variance of the process. The *f*PSD* plots in the right panels show a maximum at frequencies which are comparable to the f_{visc} (i.e. the characteristic frequency of the process). This shows that, according to the model, most of the $\dot{m}$ variations, at each ring, should operate at frequencies roughly equal to the local f_{visc}. Variations at higher and lower frequencies are dumped. At a given M_{BH}, the characteristic frequency of variations decreases with increasing distance from the central black hole. Similarly, the $\dot{m}$ variations at fixed radius, operate at lower frequencies with increasing M_{BH}.

CHAPTER 3: NUMERICAL IMPLEMENTATION OF THE MODEL

In order to study numerically the variability model that I described in the previous chapter, it is essential to discretize the disc model. Discretization implies the approximation of the accretion disc as an ensemble of concentric rings, centered around the black hole. Below, I describe the construction of the numerical code that I used in this work.

3.1 The width of the rings, Δr

First, I need to determine the width of the rings, $\Delta r_i = r_{i+1} - r_i$, where r_i and r_{i+1} are the inner and outer radii of the i^{th} ring. In the numerical code I will assume that the temperature of each ring, and hence it's luminosity, will be constant. Since the temperature depends on r, Δr should be small so that the variation of T (and L) over the width of the ring is small enough for the assumption of T (and L) being constant, to be satisfied. To this end, following ID11, I assumed that $\Delta r/r = 0.05$, i.e. the width of every ring is equal to 5% of it's inner radius. Therefore, the inner radius of each ring is defined by the equation:

$$r_{i+1} = r_i + 0.05\, r_i \quad . \quad (3.1)$$

In order to investigate whether the value of $\frac{\Delta r_i}{r_i} = 0.05$ is a reasonable choice, I wrote a program which assumes a disc with $r_{in}=6$ and $r_{out}=1000$, and consists of concentral rings with radii given by eq. (3.1). Then, I calculate the temperature $T(r_i)$ of each ring using eq. (2.7), as well as the fractional temperature difference $\Delta T(r_i)=[T(r_{i+1})-T(r_i)]/T(r_i)$. Figure (3.1) shows $\Delta T(r_i)$ as a function of r, for four different black hole masses.

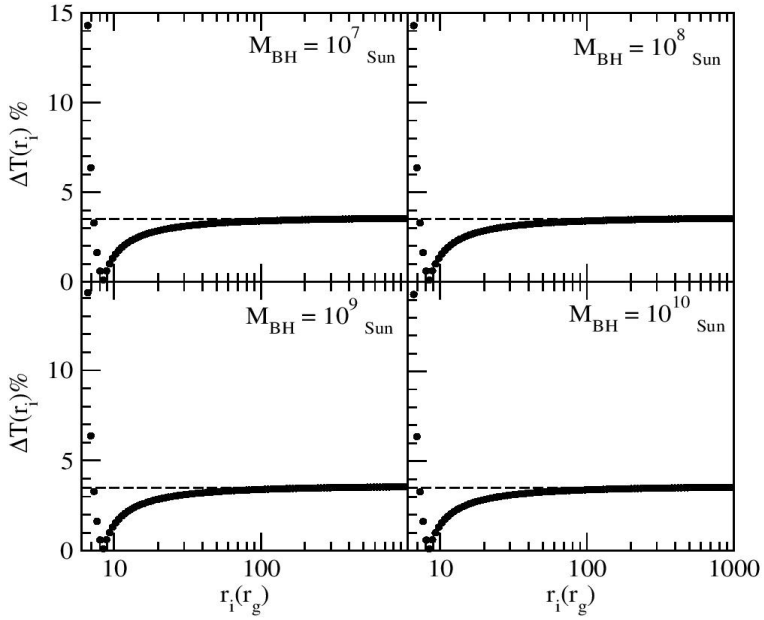

Fig. 3.1 Fractional temperature variation of the disc as a function of distance in the case of a 10^7, 10^8, 10^9 and 10^{10} M_{Sun} black hole masses (from top left to top right respectively).

The plots show that the radial dependence of $\Delta T(r)$ does not depend on M_{BH}. The temperature varies over the two innermost rings very fast. $\Delta T(r)$~15.5% for the innermost ring and ~6.5% for the next ring. For the rest of the rings, the fractional change of temperature remains less than 3.5%. For the rings around 8-10r_g, $\Delta T(r)$ drops significantly. This happens because the temperature reaches it's maximum value at these rings and $T(r)$ remains rather constant over a relatively broad range of distances. Thus, the temperature change is minimal. At distances larger than ~10r_g , the fractional temperature change per ring increases as we move further away. $\Delta T(r_i)$ reaches 3.5% at about ~100r_g and remains constant at this value at larger radii. This happens because on the outer rings, the temperature decreases at a constant rate with distance.

Therefore, I conclude that, for the given width of the rings, the temperature can be assumed as constant within each ring, except the two innermost rings. However, the contribution of these two rings to the total disc luminosity is not significant (see below), so the large temperature within these two rings should not be a big issue.

3.2 The inner and outer radii of the disc

I kept the radius of the inner ring, r_{in}, fixed at 6. This is equal to the ISCO radius for an accretion disc around a Schwarzchild black hole. However, there is no theoretical limit on the radius of the outer disc ring, r_{out}. On one hand, r_{out} needs to be large enough so that the disc model contains all rings that emit most of the radiation at the visible spectrum. On the other hand, it is essential to keep r_{out}, and hence the number of rings, as small as possible so that our calculations require the shortest time to complete.

In order to choose r_{out}, I considered the disc around a $10^7 M_{Sun}$ black hole, with r_{in}=6, r_{out}=1000, and Δr=0.05. Given these numbers, the disc is divided in 106 rings. Then, I computed the luminosity of each ring, numerically. Since the code will be used to study the optical variations as recorded by observations, I estimated the luminosity that would be recorded by a detector with the use of g_{P1}, r_{P1}, i_{P1}, z_{P1} filters. These are the filter curves used by Simm et al. (2016), whose results were reported in the Introduction. Figure (3.2) shows the filter transmission curves of these filters. The filter curves are essentially flat between λ_{min} and λ_{max} over a frequency range, say between λ_{min} and λ_{max}. Table (3.1), lists λ_{min}, λ_{max} ,the filter width $\Delta\lambda=\lambda_{max}-\lambda_{min}$, as well as the mean wavelength λ_{mean}, for each filter.

I can now estimate the luminosity of each ring as follows: since the filters are relatively narrow (with $\Delta\lambda$~150 *nm*) I assume the emitted flux at each wavelength between λ_{min} and λ_{max} is roughly equal to the flux at the mean wavelength, F_λ ($\lambda=\lambda_{mean}$), where F_λ is defined in eq. (2.8). In this case, the total luminosity of each ring (in *W*), will be roughly equal to the integral of the flux $\int_{\lambda_{min}}^{\lambda_{max}} F_\lambda(\lambda, R)d\lambda$ multiplied by the ring area $\pi\left(r_{i+1}^2-r_i^2\right)$. Since $F_\lambda(\lambda) \sim F_\lambda(\lambda=\lambda_{mean})$, this integral is approximately equal to $F_\lambda(\lambda=\lambda_{mean})\times(\lambda_{max}-\lambda_{min})$. Therefore, the total luminosity of each ring will be

$$L(r_i)=2\pi\frac{hc^2}{\lambda_{mean}^5}\frac{\pi\left(r_{i+1}^2-r_i^2\right)}{e^{\frac{hc}{k_b T_i \lambda_{mean}}}-1}(\lambda_{max}-\lambda_{min}) \quad (W). \text{ (3.2)}$$

Filter	λ_{mean} (*nm*)	λ_{min} (*nm*)	λ_{max} (*nm*)	$\Delta\lambda$ (*nm*)
g	486.6	394.3	559.3	165.0
r	621.4	538.6	703.6	165.0
i	754.5	677.8	830.4	152.6
z	867.9	802.8	934.6	131.8

Table 3.1 λ_{mean}, λ_{min} , λ_{max} and $\Delta\lambda$ values for the g_{P1}, r_{P1}, i_{P1}, z_{P1} filters (the numbers are taken from SVO Filter Profile Service, http://svo2.cab.inta-csic.es/svo/theory/fps/).

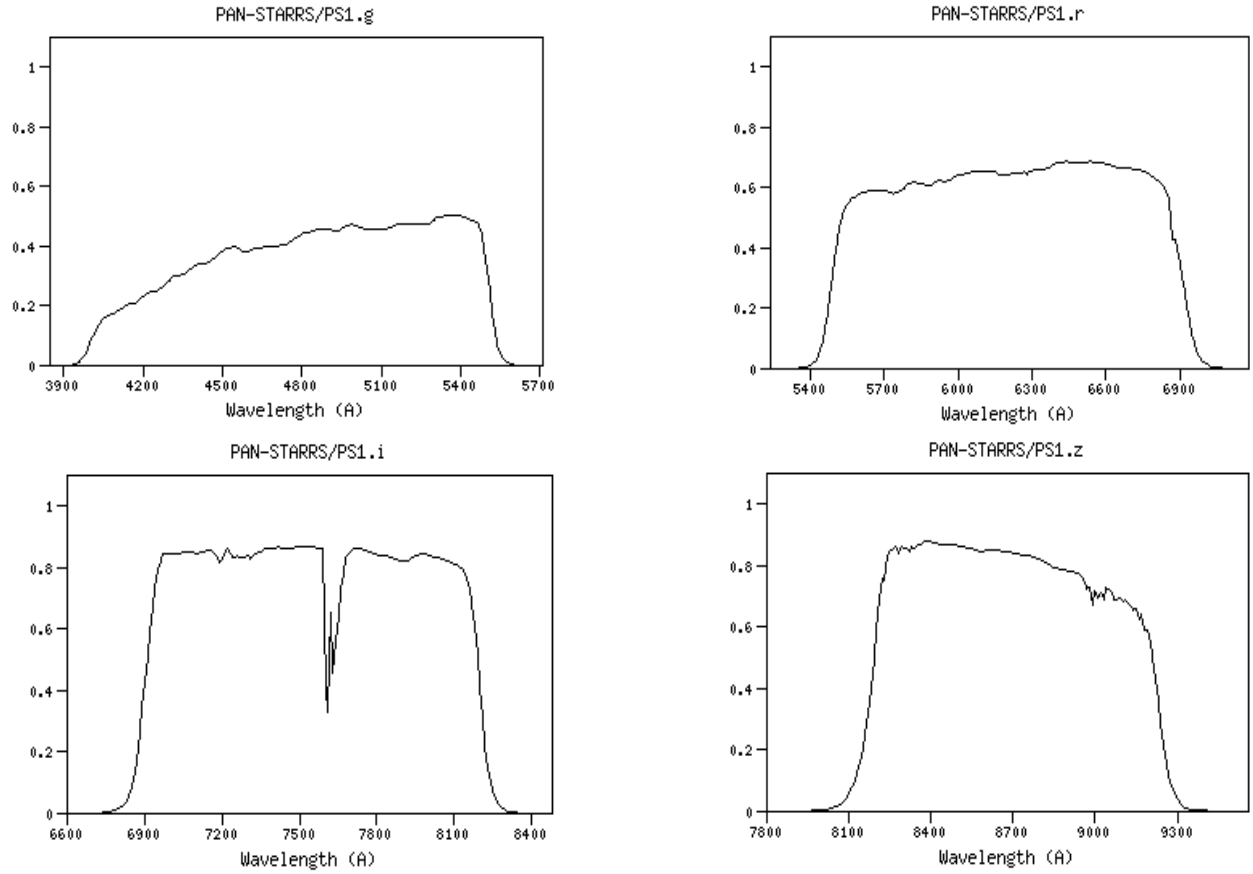

Fig. 3.2 The g_{P1}, r_{P1}, i_{P1}, z_{P1} filter transmission curves (data taken from SVO Filter Profile Service, http://svo2.cab.inta-csic.es/svo/theory/fps/).

Using eq. (3.2), I estimated the luminosity of all rings up to r_{out}=1000, for four different accretion rates, namely: 0.01, 0.05, 0.1, 0.5 of the Eddington limit (the accretion rate determines the temperature, T_i, of each ring at radius r_i ; see eq. 2.7). The results are plotted in Fig. (3.3).

This figure shows a plot of the luminosity of each ring as a function of its radius. One can see that as λ_{mean} increases (i.e. from filter g_{P1} to filter z_{P1}) the luminosity decreases, irrespective of $\dot{m}$,as expected from eq. (3.2). For all filters, the luminosity increases with increasing mass accretion rate. As eq. (2.7) dictates, the temperature increases with mass accretion rate and, following eq. (3.2), so does the luminosity (as T increases, $e^{\beta/T}$*-1* decreases, and hence L increases).

Figure (3.3) also shows that, for all filters and all accretion rates, luminosity increases with increasing radius, as r^2. This is due to the fact that the area of the rings increases with increasing radius. However, this increase stops at a certain radius, say r_{max}. This effect is more prominent in the case of the *g*-band filter luminosity plot in the top left panel of Fig. (3.3). At radii larger than r_{max} ~

400, the *g*-band luminosity decreases (for all accretion rates). In fact it becomes smaller than the luminosity of all the other filters at radii > 700. This is due to the decrease of temperature with increasing radius. Since the disc is assumed to radiate as a black body, according to the Wien's law most of the radiation from the outer radii (with lower temperature) is emitted at wavelengths which are larger than λ_{max} of the *g*-band filter. Although not shown in Fig. (3.3), the *r*-band filter luminosity will become lower than that of the *i* and *z*-band filters, and the luminosity of the *i*-band filter will become lower than that of the *z*-band filter, for even larger radii (for all mass accretion rates).

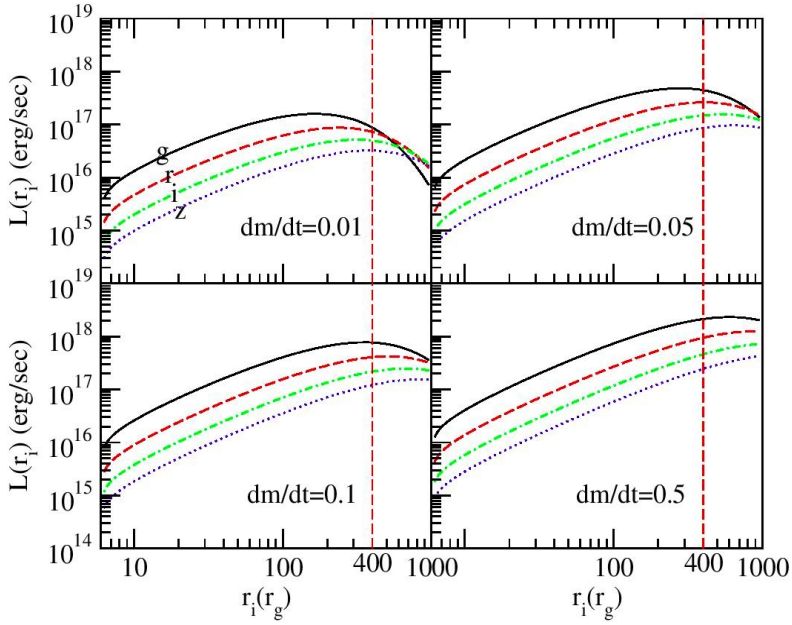

Fig. 3.3 The luminosity of the rings, plotted as a function of the ring radius for all filters, for a $10^7 M_{Sun}$ black hole. The vertical dashed line shows r_i=400.

I therefore chose to consider the outer disc radius to be $400r_g$ (i.e. r_{out} = 400). The disc emission in my numerical code should be a good approximation of the total disc emission in the *g*-band filter, as long as the accretion rate is less than 0,5 of the Eddington limit, for all black holes larger than 10^7 M_{sun}. Although not shown, $r_{max} \leqslant 400$ for larger mass black holes as well. This is because the temperature of a ring is smaller by a factor of $M_{BH}^{1/4}$ than the temperature around a $10^7 M_{Sun}$ black hole (for a given accretion rate). So, if the disc up to r_{out}=400 contributes most of the *g*-band luminosity in the case when $M_{BH}=10^7 M_{Sun}$, this is certainly the case for discs around larger black hole masses, because the rings with longer radii will be cooler for those systems, and will emit at wavelengths longer than those detected by the *g*-band filter. Since r_{in} and r_{out} are fixed, then the number of rings is also fixed: r_{in}=6, r_{out}=400 and Δr=0.05, imply that N_{rings}=86.

3.3 The $\dot{m}$ variations in each ring

Once r_{in}, r_{out} and Δr_i are fixed, the next step is to construct the random $\dot{m}$ variations at each ring, at specific times, over a certain duration (say *T*). I describe below the way I did it for each ring.

I can estimate the power spectrum of the $\dot{m}$ variations using eq. (2.17) ($\dot{m}$ refers to the mass accretion rate in units of the Eddington limit i.e. it is the Eddington ratio, see Sec. (1.4)). The amplitude of the *PSD*, as defined by eq. (2.17), is equal to one. It is necessary to define it in a proper way because it is the *PSD* amplitude that determines the amplitude of the $\dot{m}$ variations. To do so, I recall that the integral of the *PSD* (from -Inf to +Inf) is equal to the total variance of the variable process (see eq. (2.16)). Let σ_i^2 be the variance of the $\dot{m}$ variations at r_i. Then, the total variance, of all $\dot{m}$ variations of the disc will be:

$$\sigma_{tot}^2 = \sum_i \sigma_i^2 ,$$

(where the sum goes from r_{in} to r_{out}), if the $\dot{m}$ variations in any one ring are independent from the variations in the other rings. I further assumed that the variations at each ring contribute by the same factor to σ_{tot}^2, therefore,

$$\sigma_i^2 = \sigma_{tot}^2 / N_{rings} \quad . (3.3)$$

I defined the amplitude of the *PSD*, at each ring r_i, as

$$PSD_{norm,i} = \frac{\sigma_i^2}{\pi f_{visc}(r_i)} = \frac{\sigma_{tot}^2 / N_{rings}}{\pi f_{visc}(r_i)} \quad , (3.4)$$

so that the integral of the $PSD(f_i)$, from -Inf to +Inf, will be equal to σ_i^2, since the integral of the *PSD*, as defined by eq. (2.16), from -Inf to +Inf, is equal to $\pi f_{visc}(r_i)$. Having normalized the *PSD* properly, I can now produce $\dot{m}$ variations following the Timmer and Koenig method (Timmer & Koenig, 1995).

According to this method, first I estimate the *PSD* at a particular set of frequencies which depends on the number of points and the duration of the time series of the $\dot{m}$ variations. If I wish to estimate $\dot{m}$ at *N* time points which are equally spaced by Δt, the *PSD* must be calculated at a set of frequencies defined by

$$f_i = \frac{i}{N\Delta t} \quad , (3.5)$$

where *N* is the number of points in the time series ($N \cdot \Delta t = T$,) and $i = 0, +/-1, \ldots, +/-N/2$. At zero frequency, the *PSD* value is equal to the mean of the $\dot{m}$ variations. At positive frequencies, the *PSD* is estimated using eq. (2.17), with the normalization defined in eq. (3.4). At negative frequencies: $PSD(-f_i) = PSD(f_i)$. Having defined the *PSD* in this way, the method uses the inverse-Fourier transform to estimate the $\dot{m}$ values at $t_i = \Delta t, 2\Delta t, \ldots, N\Delta t$.

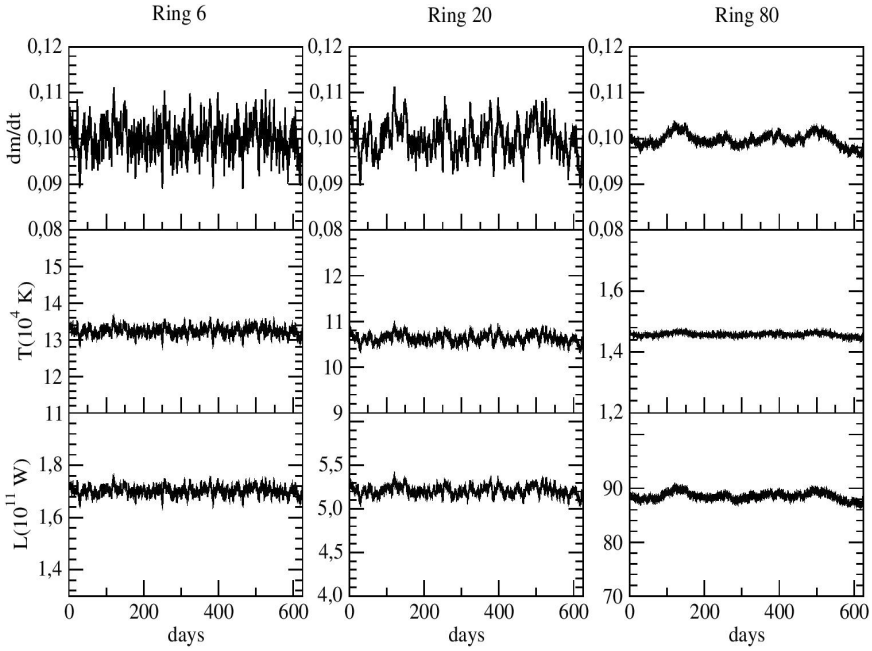

Fig. 3.4 Mass accretion rate, temperature and luminosity fluctuations at rings 6, 20 and 80, around a $10^7 M_{Sun}$ black hole mass (from the top to the bottom panels, respectively). The time series duration is *T*=625 *days*.

As an example, the top panels in Fig. (3.4), show the $\dot{m}$ variations that I constructed for the disc rings at r_i = 6, 20 and 80. I assume $M_{BH}=10^7 M_{sun}$, $\sigma^2_{tot}=0.1$, $\sigma^2_i=0.1/N_{rings}$ and $\dot{m}=0.1$ (N_{rings}=86, as explained above).

3.4 The luminosity variations in each ring

The main aim is to predict the disc luminosity variations (as this is what we observe). Therefore, I used the $\dot{m}$ time series to estimate the temperature variations at each ring. To this end, I used eq. (2.7). In the middle panel of the same figure, I show the temperature variations calculated in this way. Having defined the temperature of each ring as a function of time, I used eq. (3.2) to estimate the ring luminosity at each time. In the bottom panels of Fig. (3.4) I show the resulting luminosity variations of each ring.

Ring	$f_{rms.\dot{m}}$	$f_{rms,T}$	$f_{rms,L}$	t_{visc} (*Days*)
6	0.035	0.009	0.009	12
20	0.035	0.008	0.009	33.5
80	0.013	0.003	0.007	2708

Table 3.2 Fractional root mean square variability of the physical quantities plotted in Fig. (3.4).

The *max/min* ratio in the *y*-axis is kept the same at all panels of Fig. (3.4). In this way, it is easy to compare, by eye, the amplitude of the variations in each panel. It seems that the variability amplitude of all quantities is similar in the two inner rings, but decrease in the outer ring. Also, the amplitude of the temperature and luminosity variations is smaller than the accretion rate variations, for all rings.

To quantify this difference, I estimated the so-called "fractional root mean square variability amplitude" (f_{rms}) of each time series plotted in Fig. (3.4). f_{rms} is defined as the ratio of the average scatter of the points around the mean (i.e. the standard deviation of the time series) over the mean. I list the results in Table (3.2).

By construction, the standard deviation of the accretion rate variations in each ring should be $\sqrt{0.1/86}=0.034$. Since the original mean of the $\dot{m}$ variations was equal to one, then $f_{rms,\dot{m}}=0.034$ (the fact that I multiplied the resulting $\dot{m}$ values with 0.1 does not affect this number, as both the standard deviation and the mean of the resulting time series are affected by the same factor, in the same way). The results indicate a decrease of $f_{rms,\dot{m}}$ for the outer ring. This is expected as I will explain later.

However, $f_{rms,T}$ and $f_{rms,L}$ are smaller than $f_{rms.\dot{m}}$ at all rings. Regarding the difference between $f_{rms,T}$ and $f_{rms,\dot{m}}$, this is due to the fact that the mass accretion rate appears to the 1/4th power in eq. (2.7). As a result, a $\Delta\dot{m}$ variation should result in a ΔT variation such that, $\frac{\Delta T}{T}\sim\frac{1}{4}\frac{\Delta\dot{m}}{\dot{m}}$. Indeed, $f_{rms,T}\sim 0.25$ in $f_{rms,\dot{m}}$ at all rings (see Table (3.2)).

On the other hand, $f_{rms,T}$ and $f_{rms,L}$ are similar in the inner rings, but the temperature variations appear to be less than ~ 3 times smaller than the luminosity variations in the outer ring. To investigate this, I calculate a derivative of L with respect to T. For simplicity, eq. (3.2) can be written as,

$$L(r_i) = A \frac{1}{e^{\frac{hc}{\lambda k_B T(r_i)}} - 1} \quad , (3.6)$$

where *A* is a constant. Then if I differentiate $L(r_i,)$ with respect to *T*, I get

$$\frac{dL}{dT} \propto \frac{\beta}{T^2} \frac{e^{\beta/T}}{(e^{\beta/T} - 1)^2} \quad ,$$

where $\beta = \frac{hc}{\lambda k_B}$. Now, if I divide the equation above with eq. (3.6), I get the following equation for small variations of *L* and *T* around their mean values:

$$\frac{\Delta L}{L} \simeq \frac{\beta}{T} \frac{e^{\beta/T}}{[e^{\beta/T} - 1]} \frac{\Delta T}{T} \quad . (3.7)$$

The above equation is valid under the assumption that the temperature remains constant over the width of each ring. The temperature at rings 6 and 20 are $11 \times 10^4 K$ and $9 \times 10^4 K$, respectively (for the M_{BH} and $\dot{m}$ values of $10^7 M_{Sun}$ and 0.1, respectively). Using the above equation and these values I find that $\Delta L/L \sim \Delta T/T$, in agreement with the results listed in Table (3.2). However, at the outer ring, $T \sim 1.25 \times 10^4 K$. For this temperature, $\frac{\beta}{T} \frac{e^{\beta/T}}{[e^{\beta/T} - 1]} \sim 3$, and so $\Delta L/L \sim 3\Delta T/T$, in agreement with the results of Table (3.2) for this ring.

3.5 Propagation of mass accretion rate fluctuations

The previous sections describe how the numerical code computes random luminosity variations, over specified time intervals, at each ring. However, the main goal is to predict the luminosity variations of the whole disc. In order to do so, I need to take into account one more basic feature of the model: the propagation of the accretion rate variations from the outer to the inner rings.

Let us suppose that the mean mass accretion rate in the outermost ring is equal to $\dot{M}_0$. According to the model, the accretion rate variations in this ring will be :

$$\dot{M}_{out}(t) = \dot{M}_0 \dot{m}_{out}(t) \quad , (3.8)$$

where $\dot{m}_{out}$ are the random variations I calculate as explained in Sec. (3.3). $\dot{M}_{out}(t)$ will then propagate inwards, traveling a distance equal to the width of the outer ring, Δr_{out} , at a certain time, say *tlag(out)*. In general, the time needed for an accretion rate fluctuation to travel across the width of the i^{th} ring is equal to the ratio of the width of the ring over the radial speed of the inward movement of the fluctuation, i.e.

$$tlag(i) = \frac{\Delta r(i)}{\upsilon(i)} \quad ,$$

where, *Δr(i)* is the width of the ring, and $\upsilon(i) = r_{i+1} fvisc(r_{i+1})$ (*days*$^{-1}$) is the radial speed at the outer radius of the ring. Therefore, the propagation time over the i^{th} ring will be:

$$tlag(i)=\frac{[r_i\times 0.05]}{[r_{i+1} fvisc(r_{i+1})]} \quad (days), \text{ (3.9)}$$

where $i = 2, \ldots 86$. So, $\dot{M}_{out}(t)$ will have reached the next ring at time $t'=t+tlag(out)$, and the mass accretion rate for this ring, at time t', will be:

$$\dot{M}_{out-1}(t')=\dot{M}_{out}(t)\dot{m}_{out-1}(t') \quad . \text{(3.10)}$$

The above equation can also be written as:

$$\dot{M}_{out-1}(t)=\dot{M}_{out}[t-tlag(out)]\dot{m}_{out-1}(t) \quad , \text{ (3.11)}$$

which is valid at all times, t. Generalizing the above equation, the mass accretion rate at any ring (except from the outer ring) will be:

$$\dot{M}_i(t)=\dot{M}_{i+1}[t-tlag(i+1)]\dot{m}_i(t) \quad , \text{(3.12)}$$

where $i=1, \ldots, 85$. For the outer ring, the accretion rate variations are given by eq. (3.8). Equation (3.12) can also be written as follows,

$$\dot{M}_i(t)=\dot{M}_0 \prod_{j=i}^{Nrings} \dot{m}_j(t_j) \quad , \text{(3.13)}$$

where $t_j=t$, when $j=i$, and

$$t_j=t-\sum_{k=i+1}^{j} tlag(k) \quad , \text{ (3.14)}$$

when $j>i$, $tlag(k)$ in eq. (3.14) is given by eq. (3.9). Equations (3.12) or (3.13) can be used to determine the accretion rate at each ring of the disc, at any time t, provided that past accretion rate fluctuations in the outer rings are also known. The final step is to decide at which time points $\dot{m}$ variations will be calculated.

<u>Determination of Δt:</u> Let us assume that we wish to estimate accretion rate variations in the inner ring (i.e. ring 1) at times

$$t_1(i)=i\times\Delta t, i=1,2,\ldots,n_p \quad ,$$

where n_p is the number of points, and the duration of the time series will be $T=n_p\Delta t$. According to eq. (3.12), in order to take into account the propagation of fluctuations, the $\dot{m}$ variations in the ring just outside the inner ring (i.e. ring 2) must be computed at,

$$t_2(i)=i\times\Delta t, i=-tlag(2)/\Delta t, \ldots, 1,2,\ldots,n_p \quad . \text{(3.15)}$$

If Δt is larger than $tlag(2)$, then the calculation of the $\dot{m}$ variations in the inner ring will not be accurate. The variations will have smaller amplitude than expected, because the $\dot{m}$ values at each time point will be an average of the true $\dot{m}$ variations over the broad bin size Δt. We therefore define Δt as follows:

$$\Delta t = \frac{tlag(2)}{2} \quad (days) \text{ or}$$

$$\Delta t = 1 \quad (day) \text{ if} \quad \frac{tlag(2)}{2} > 1 \quad (day). \quad (3.16)$$

In summary, for a given time duration of the time series, *T* the code:

1) computes *tlag(i)* from ring 2 to the outer ring *(i*=86*)*, using eq. (3.9).

2) computes Δt from eq. (3.16).

4) computes the total number of points in the time series: $n_p = T/\Delta t$.

5) computes the $\dot{m}$ variations (as explained in Sec. (3.3)) of the outer ring, for a total number of points n_p. Then computes the mass accretion rate of this ring for a total number of points of

$$n_{i=86} = n_p + \sum_{j=2}^{86} \frac{tlag(j)}{\Delta t} \quad \text{, using eq. (3.8).}$$

6) computes the $\dot{m}$ variations (as explained in Sec. (3.3)) for all rings in a number of points of $n_i = n_p + \sum_{j=2}^{i} \frac{tlag(j)}{\Delta t}$ and the accretion rate variations using eq. (3.12) until the innermost ring. For the inner ring, $n_1 = n_{out}$.

3.6 The resulting $\dot{m}$ variations, when considering propagation

Figure (3.5) shows a plot of the mass accretion rate variations at ring 20 estimated without assuming propagation of mass accretion rate fluctuations from the outer rings (upper panel) and when I take into account this propagation from the outer rings (bottom panel). I have assumed $M_{BH} = 10^7 M_{sun}$, and $\dot{M}_0 = 0.1$ (in both cases).

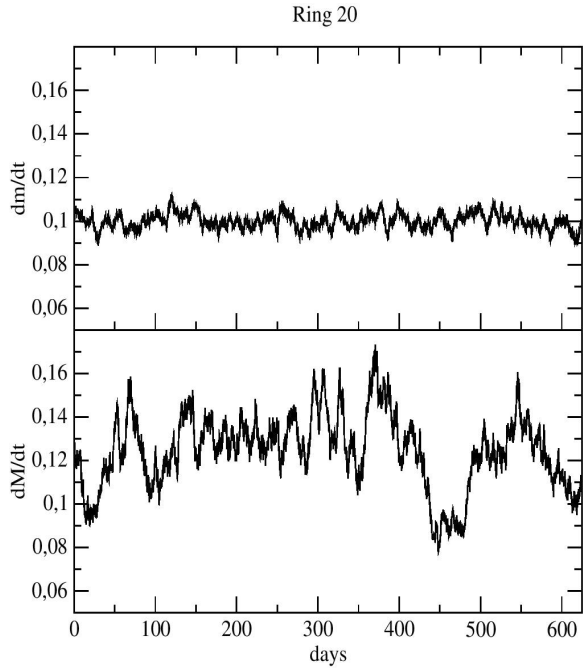

Fig. 3.5 Mass accretion rate variation of ring 20, without/with taking into account $\dot{M}$ propagation of the fluctuations (top and bottom panels, respectively).

The plot in the top panel of Fig. (3.5) and in the the upper middle panel of Fig. (3.4) are the same. The most significant difference between the $\dot{M}$ variations when we consider the propagation of variations from the outer rings is that large amplitude, long term variations appear, and the variability amplitude increases. I computed the fractional variability for the time series plotted in the top and bottom panels of Fig. (3.5) and I found: $f_{rms.\dot{M}}=0.035$ and $f_{rms.\dot{M}}=0.135$, respectively. The increased amplitude of the $\dot{M}$ variations is due to the fact that the $\dot{m}$ variations in each ring are also affected by variations at bigger radii, which last longer. We can predict the variance of the $\dot{m}$ variations in each ring as follows:

According to eq. (3.13) the mass accretion rate at $r=r_i$, $\dot{M}_i(t)$, is a random variable which is equal to the product of $\dot{m}$ variations in the N_{rings}-i outer rings, which are propagated inwards. These random variables are independent. To estimate $\sigma^2[\dot{M}_i(t)]$, let us consider a random variable, say *Y*, which is the product of *n* random variable values x_i , i.e.

$$Y=\prod_1^n x_i \quad .$$

Then,

$$\sigma^2(Y)=E[(x_1\cdots x_n)^2]-E^2(x_1\cdots x_n) \quad .$$

Using the properties of the mean value of a product of *n* independent random variables, the above equation can be written as:

$$\sigma^2(Y)=\prod_1^n E[x_i^2]-\prod_1^n E^2[x_i] \quad ,$$

and, using the fact that $\sigma^2(x_i)=E[x_i^2]-E^2(x_i)$ I get,

$$\sigma^2(Y)=\prod_1^n [\sigma^2(x_i)+E^2(x_i)]-\prod_1^n E^2[x_i] \quad .$$

In our case, for the accretion rate variations at ring *i*, $Y=\prod_{j=i}^{86}\dot{m}_j(t_j)$, so

$$\sigma^2(Y)=\prod_{j=i}^{86}\{\sigma^2[\dot{m}_j(t_j)]+E^2[\dot{m}_j(t_j)]\}-\prod_{j=i}^{86}E^2[\dot{m}_j(t_j)] \quad . \quad (3.17)$$

Since $\dot{M}_i(t)=\dot{M}_0\prod_{j=i}^{86}\dot{m}_j(t_j)$, then

$$\sigma^2[\dot{M}_i(t)]=\dot{M}_0^2\cdot\sigma^2[\prod_{j=i}^{86}\dot{m}_j(t_j)]=\dot{M}_0^2\cdot\prod_{j=i}^{86}\{\sigma^2[\dot{m}_j(t_j)]+E^2[\dot{m}_j(t_j)]\}-\dot{M}_0^2\cdot\prod_{j=i}^{86}E^2[\dot{m}_i(t_i)] \quad . (3.18)$$

In our case, $E[\dot{m}_i]=1$ and $\sigma^2(\dot{m}_i)=1.16\times10^{-3}$, for every *i*. Therefore, the above equation reduces to:

$$\sigma^2[\dot{M}_i(t)]=\dot{M}_0^2\cdot[(1.16\times10^{-3}+1)^{(87-i)}-1] \quad . (3.19)$$

Figure (3.6) shows the variance of the mass accretion rate fluctuations at each disc ring (from i=1 to 86), while considering propagation of the $\dot{m}$ fluctuations from the outer rings. To compute $\sigma^2(\dot{M})$, I considered a disc around a black hole of $10^7 M_{Sun}$, $\dot{M}_0$=0.1, and I created a time series for the $\dot{m}$ fluctuations in each ring with $\sigma^2_{tot}=0.1, \sigma^2(\dot{M})=1.16\times10^{-5}, T=625\,days$, and $\Delta t=0.125\,days$. I used the data of these time series to compute the variance of the $\dot{m}$ fluctuations at each ring, which I plotted with up-triangles in Fig. (3.6).

The solid horizontal line in Fig. (3.6) indicates the variance of the $\dot{M}$ fluctuations in each ring (without any propagation effects), which by construction is equal to 0.034, at all rings. Obviously, the observed variance is larger than this value at almost all rings.

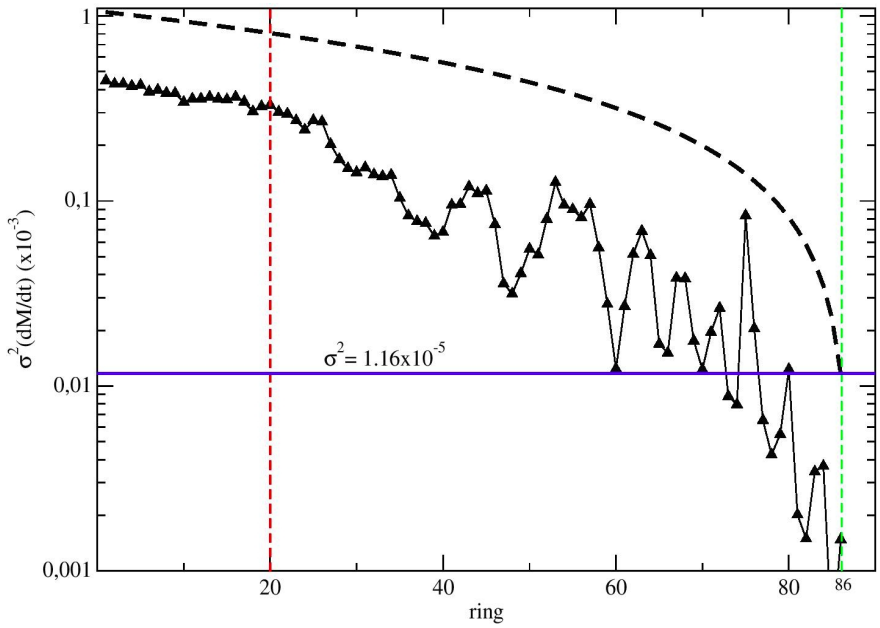

Fig. 3.6 The variance of $\dot{M}$ variations at each ring when I consider propagation of $\dot{m}$ fluctuations from the outer rings (up-triangles). The left and right dashed vertical lines indicate rings 20 and 86, respectively. The solid horizontal line shows the variance of the $\dot{M}$ variations in each ring in the absence of $\dot{m}$ propagations. The black dashed line represents the theoretical variance of each ring estimated using eq. (3.19).

The dashed line shows the expected variance of the $\dot{M}$ variations, computed using eq. (3.19). Clearly, the variance of each ring when computed using the data from the simulated time series is smaller than the predicted variance. The variance becomes smaller than that of a single ring at rings further away from the ~70th ring.

I believe that the reason for the underestimation of the variance is due to the fact that the total duration of the $\dot{m}$ time series is finite. As a result, longer variations do not have time to develop and reach their maximum amplitude in order to fully contribute to the total variance. For example, the expected value of $\sigma^2_{\dot{M}}$ for the outermost ring, as calculated using eq. (3.19), is equal to that of a single ring in the absence of propagations (notice that the dashed line in Fig. (3.6) intercepts the horizontal solid line at ring 86). However, eq. (3.19) gives $\sigma^2_{\dot{M}}$ in the case of an infinite lightcurve, i.e. $\sigma^2_{\dot{M}}$ in this equation is equal to the *PSD(f)* integral is form 0 to Infinity. In my case T=625 *days*, so the measured $\sigma^2_{\dot{M}}$ should be only an estimation of the *PSD(f)* integral from 1/625 *days*$^{-1}$ to Infinity, which is smaller than the value of the *PSD(f)* integral from 0 to Infinity.

Figure (3.7) shows the viscous timescale as a function of ring radius for a 10^7 M_{Sun} (continuous line). The horizontal dashed line indicates the duration of the $\dot{M}$ time series that I created. After ~ ring 40, the viscous timescale becomes longer than the total duration of the lightcurve. The viscous frequency is the breaking point for the *PSD(f)* function at each ring. Therefore, the fact that $t_{visc} \geq T$ at rings $i \geq 40$, can explain that the variance that I measure is smaller than what eq. (3.19) predicts.

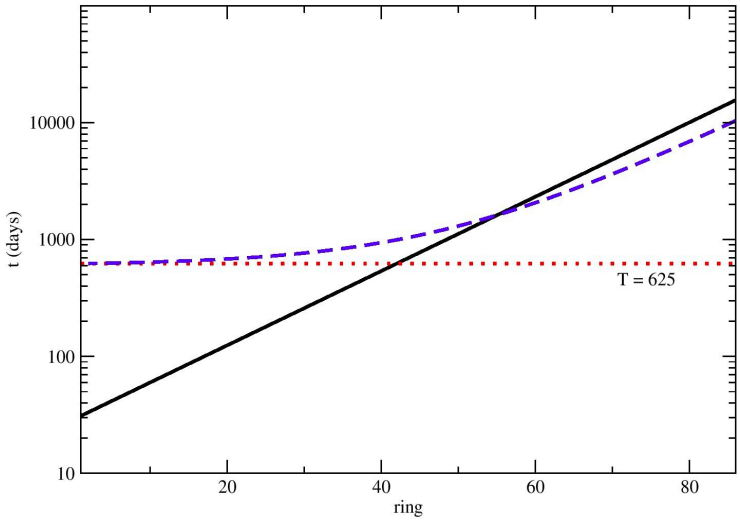

Fig. 3.7 The viscous timescale, t_{visc}, as a function of radius for a 10^7 M_{Sun} (continuous line). The horizontal dashed line shows the lightcurve duration of 625 *days*.

However, for the innermost rings (where $t_{visc} \leqslant T$), the *PSD(f)* integral from 1/625 $days^{-1}$ up to infinity should be roughly equal to the integral from 0 to Infinity. Contrary to this, the observed variance of the $\dot{M}$ variations is smaller than what is theoretically predicted.

The variations of the inner rings are affected by the variations of the outer rings that have reached them through propagation. The dashed line in Fig. (3.7) indicates the time that is needed for the accretion rate fluctuations to propagate from the i^{th} to the innermost ring. To take into account the propagation effects to the inner rings correctly, I must calculate the $\dot{m}$ variations in the outer ring over a period which is significantly longer than T but smaller than t_{visc}. Therefore, the low frequency, large amplitude variations that reach the inner rings are not fully developed and this results in a loss of variability.

3.7 The final lightcurve

After I have calculated numerically $\dot{M}(r_i, t)$ at each ring, I can now use eq. (2.7) to find the temperature of each ring as a function of time, $T(t_i)$, and then eq. (3.2) (with the values of λ_{max}, λ_{min}, λ_{mean}, for the g_{P1} filter, taken from Table (3.1)) to find the lightcurve of each ring, $L(t_i)$. The total luminosity of the accretion disc at each time t is equal to:

$$L_{disc}(t) = \sum_{i=1}^{N} L(r_i, t) \quad . (3.20)$$

Figure (3.8) shows the output of the code for a black hole mass of $10^7 M_{Sun}$, with a mean mass accretion rate of 0.1 of the Eddington ratio, $\sigma_{\dot{m}}^2 = 0.1$ and a duration of 625 *days*.

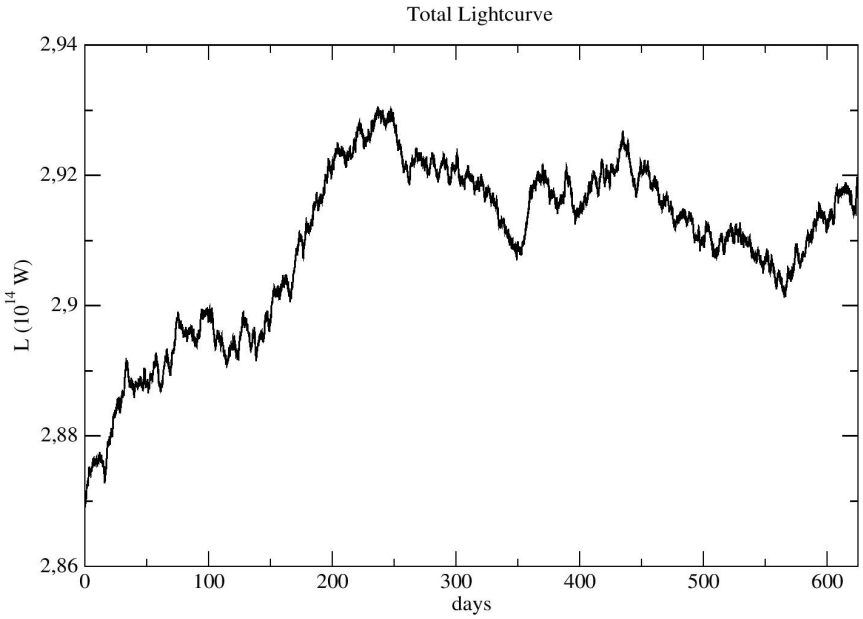

Fig. 3.8 *g*-band lightcurve of a $10^7 M_{Sun}$ black hole mass object, with a mean mass accretion rate of 0.1 of the Eddington ratio, $\sigma_{\dot{m}}^2 = 0.1$ and a duration of 625 *days*.

The luminosity's fractional root mean square variability, $f_{rms,L,total} = 0.004$,is similar to the value of $f_{rms,L}$ for rings 6, 20 and 80 in the absence of propagations (see Sec. (3.4)). However, just like the variability amplitude (normalized to the mean) of the accretion rate fluctuations in a ring increases when we consider propagation, the same is true with the variability amplitude of the luminosity variations. In fact, $f_{rms,L} = 0.07, 0.07,$ and 0.01, for rings 80, 20 and 6 respectively, when I consider the propagation effects. These numbers are larger than the variability amplitude of the luminosity variations without propagation. But it is also significantly larger than f_{rms} of the luminosity variations of the whole disc, even when I consider propagation of the $\dot{m}$ variations. This is due to the fact that the normalized standard deviation of the sum of N independent variables will be smaller (at least by) a factor of $1/\sqrt{N}$, i.e. by a factor of 10, in our case.

CHAPTER 4:
SUMMARY AND CONCLUSIONS

In this work, I developed a numerical code that can produce a variable light curve for an AGN in any optical/UV band. The code has the following input:

-Inner and outer radii of the accretion disc (r_{in} and r_{out}, respectively), measured in gravitational radii (r_g), as explained in Chapter 3. The width of the disc ring is fixed at $\Delta r=0.05r$.

-Black hole mass, and accretion rate in units of the Eddington accretion rate.

-The total variance, of the $\dot{m}$ variations which determines the power spectrum amplitude.

As long as the above input values are determined, the code can produce time series of: $\dot{m}$ and T variations at each ring, and L variations at each ring, as well as of the whole disc. The resulting time series can last any duration T, while the bin size is determined as explained in Sec. (3.5). The disc luminosity variations can be calculated in any optical/UV bands, as long as the maximum and minimum wavelength of the band is determined. As it is now, the code assumes a constant response of the "filter" that is considered.

4.1 Assumptions and future developments

The code was developed under certain assumptions, in order to achieve simplicity and low debugging time. In its current form, the model assumes that the radiation mechanism consists only of local heating due to accretion power being locally dissipated, as dictated by virial theorem. It also assumes that the temperature is constant over the width of each ring and that the filter response curve is constant. These two assumptions allow for the simple calculation of the flux and luminosity, avoiding integrals. This reduces drastically the debugging period when computational resources are limited.

The accretion disc follows the thin disc approximation and extends from 6 to 400 gravitational radii, around a non rotating black hole. The r_{in} is the radius of the ISCO and r_{out} was chosen in such a way so that the model correctly estimates the full disc emission in the *g*-band filter. In the future, I should develop the code so that it automatically determines r_{max}, for any given optical/UV band filter. I should also develop a subroutine to calculate the disc luminosity, taking into account the true response curve of any filter.

A major development would be to also consider X-ray irradiation of the disc. This will require a significant change in the code. First of all, I will have to take into account that just a fraction of the accretion power can be dissipated locally into heating the disc while the rest is transferred into heating the X-ray source. The theoretical treatment of the disc temperature profile in this case has already be done by Svensson & Zdziarski, (1994). I will need to change this profile by assuming a particular geometry for the X-ray source that will illuminate the disc. The easiest geometry is that of a "lamp-port", i.e. the X-ray source is a point-like source, located at the center of the disc at a height h above the black hole. In this case, it will be possible to calculate the amount of radiation that illuminates each disc ring. Then, I will add this to the locally generated power and re-calculate, self consistently, the new temperature profile of the disc.

4.2 Usage of the code

The code can be executed multiple times over a range of different inputs like, for example, the black hole mass and mean mass accretion rate. In this way, I will be able to test the model predictions with the optical variability results that have been presented during the last few years. For example, in the Introduction I mentioned the results of Simm et al (2016). These authors observed a large number of AGN and studied the correlation between the optical variability amplitude versus the black hole mass, the Eddington ratio and the luminosity of the objects in their sample. If I wish to compare the model predictions with their results, then I will have to run the code for as many times as the number of the objects in their sample. The code will run for a range of black hole mass and Eddington ratio values that will be representative of the respective values in their sample. Then: *i)* I will calculate the variance of the light curves I will produce, *ii)* I will plot variance as function of black hole mass, Eddington ratio and luminosity (just like Simm et. al (2016) did), *iii)* will fit the data with a straight line, and I will compare the best fit parameter values with Simm's et. Al (2016) results. In this way, I will be able to investigate whether the model is consistent with observations and, if yes, what is the necessary $\dot{m}$ variability amplitude for this.

Also the code, as it is now, possibly predicts time lags between lightcurves of different wavelengths that are in the opposite way than the ones observed in AGN. According to the model, the luminosity variations at shorter wavelengths should appear to be delayed compared to the luminosity variations at longer wavelengths, since the mass accretion rate fluctuations begin in the outer ring and then propagate towards the inner rings that are characterized by higher temperatures. However, such a study must be delayed until the X-ray irradiation mechanism is implemented in the code. In this way, it will be possible to investigate what are the necessary physical conditions (i.e. amount of the generated power transferred to the X-ray source, amplitude of the $\dot{m}$ variations etc.) for the X-ray irradiation induced time lags to overcome the intrinsic, $\dot{m}$ fluctuations generated time lags.

References

- Rosswong, S., Bruggen, M. (2007). *Introduction to High-Energy Astrophysics*. Cambridge University Press.
- Giveom, U., Maoz, D., Kaspi, S., Netzer, H. and Smith, P.S. (1999) *Monthly Notices of the Royal Astronomical Society,* 306, 637
- Vanden Berk, et. al (2004) *The Astrophysical Journal,* 601, 692
- Hook, I.M., McMahon, R.G., Boyle, B.J. and Irwin, M.J. (1994) *Monthly Notices of the Royal Astronomical Society,* 268, 305
- Wilhite, B.C., Brunner, R.J., Grier, C.J., Schneider, D.P. and Vanden berk, D.E. (2008) *Monthly Notices of the Royal Astronomical Society,* 383, 1232
- Bauer, A. et. al 2009, *The Astrophysical Journal,* 705, 46
- MacLeod, C.L. et. al (2010) *The Astrophysical Journal,* 721, 1014
- Zuo, W., Wu, X.B., Liu, Y.Q. and Jiao, C.L. (2012) *The Astrophysical Journal,* 758, 26
- Wold, M., Brotherton, M.S. and Shang, Z. (2007) *Monthly Notices of the Royal Astronomical Society,* 375, 989
- Simm, T. et. al (2016) *Astronomy & Astrophysics,* 585, 23
- Ai, Y.L. et. al (2010) *The Astrophysical Journal Letters,* 716, 31
- Edelson, R. et. al (2015) *The Astrophysical Journal,* 806, 14
- Lyubarskii, Yu., E. (1997) *Monthly Notices of the Royal Astronomical Society,* 292, 679
- Arevalo, Uttley, P. (2006) *Monthly Notices of the Royal Astronomical Society,* 372, 401
- Ingram, A., Done, C. (2011) *Monthly Notices of the Royal Astronomical Society,* 415, 2323
- Pringle, J.E. (1981) *Annual review of astronomy and astrophysics, 19*. (A82-11551 02-90) Palo Alto, CA, Annual Reviews, Inc., 1981, 137
- Timmer, J. Koenig, M. (1995) *Astronomy and Astrophysics,* 300, 707
- Czerny, B. (2006) *AGN Variability from X-Rays to Radio Waves ASP Conference Series, 360*, San Francisco: Astronomical Society of the Pacific, 265
- Shakura, N.I., Sunyaev, R.A. (1973)
- Svensson, R., Zdziarski, A.A. (1994) *Astrophysical Journal,* 436, 599